Automated pathologies detection in retina digital images based on complex continuous wavelet transform phase angles

Salim Lahmiri, Christian S. Gargour, Marcel Gabrea

Department of Electrical Engineering, École de technologie supérieure, Montréal, Québec, H3C 1K3, Canada
E-mail: marcel.gabrea@etsmtl.ca

Published in Healthcare Technology Letters; Received on 16th May 2014; Revised on 22nd September 2014; Accepted on 29th September 2014

An automated diagnosis system that uses complex continuous wavelet transform (CWT) to process retina digital images and support vector machines (SVMs) for classification purposes is presented. In particular, each retina image is transformed into two one-dimensional signals by concatenating image rows and columns separately. The mathematical norm of phase angles found in each one-dimensional signal at each level of CWT decomposition are relied on to characterise the texture of normal images against abnormal images affected by exudates, drusen and microaneurysms. The leave-one-out cross-validation method was adopted to conduct experiments and the results from the SVM show that the proposed approach gives better results than those obtained by other methods based on the correct classification rate, sensitivity and specificity.

1. Introduction: Automatic digital image processing systems are becoming increasingly important in health care, since they allow efficient processing of images and objective medical diagnostics. In recent years, a particular interest has been devoted to the design of an automated computer-based system for the screening of retina digital images [1] to detect the presence of exudates [2, 3], drusen [4, 5] and microaneurysm (MA) [6, 7]. In the problem of exudates detection [2]; contrast enhancement fuzzy C-means and support vector machines (SVMs) were used to detect and classify bright lesions. The obtained sensitivity and specificity were 88 and 84%, respectively. Multi-scale morphological algorithms were used in [3] for exudate detection, to obtain a sensitivity of 95.0% and a specificity of 84.6%. In the problem of drusen detection, template matching and region growing were adopted in [4] to detect the suspicious area. The proposed system achieved a sensitivity of 83%. A gradient-based segmentation algorithm based on labelling the maximum gradient path was adopted in [5] to isolate drusens. Then, they were fitted by Gaussian functions to compute the area affected. The sensitivity and specificity for the automated process were 0.664 and 0.963, respectively. In the problem of MA detection, a multiscale amplitude modulation frequency modulation approach was followed in [6] for the instantaneous characterisation of normal and pathological retinal structures. Using partial least square, the automated diagnosis system achieved a sensitivity of 92% and a specificity of 54%. In [7], the problem of MA detection was formulated as a detecting target problem in which the target is embedded in a background clutter. The SVM [8] with radial basis function kernel achieved a sensitivity of 0.90 on one database and 0.45 on the other at a specificity of 0.90. A comprehensive review on the subject can be found in [1].

In this Letter, we present a new automated retinal pathologies detecting system based on the analysis of retina image by means of the complex continuous wavelet transform (CCWT) [9, 10]. The CCWT will be used here because it allows the detection of local singularities in the signal, it is shift invariant and provides good directional selectivity. The complex wavelet transform provides information about the magnitude, as well as about the phase angle of the analysed signal. It continuously decomposes the signal into the magnitude and the phase angle. The magnitude describes the strength of the local variations, while the phase angle indicates their location. In our automated retinal diagnosis system, only information about the phase angle will be considered to characterise the image. Unlike the magnitude of a complex valued image, the phase image is not affected by colour variation, non-uniform illumination and intensity variations. In addition, the phase image reflects the geometrical structure of this image.

This Letter is organised as follows: Section 2 describes the proposed method; in Section 3, the simulation results are presented; finally, Section 4 gives the conclusion.

2. Methodology: The complex continuous Gaussian wavelet transform is chosen based on two assumptions. First, we make the hypothesis that the biological texture of the retina is normally distributed. Thus, large deviations from this hypothesis could characterise abnormal images. Second, the complex continuous Gaussian wavelet is appropriate to detect local variations in the signal because of its smoothness.

The CWT of a square integrable function (signal) $s(t)$ where $s(t) \in L^2(\mathrm{R})$ is given by [9]

$$W(a, b) = \frac{1}{\sqrt{|a|}} \int s(t) \psi\left(\frac{t-b}{a}\right) \mathrm{d}t \tag{1}$$

where a and b denote the scale and translation parameters, $W(a, b)$ are the wavelet coefficients and $\Psi(t)$ is the mother wavelet function. The complex Gaussian wavelet $\Psi_G(t)$ – which is the mother wavelet in our case – is given by

$$\psi_G(t) = C_p \cdot \mathrm{e}^{-t^2} \cdot \mathrm{e}^{-jt} \tag{2}$$

where C_p is a scaling parameter and $j = \sqrt{-1}$. Then, the instantaneous phase angle $\phi(a,b)$ of $W(a, b)$ is calculated as follows

$$\phi(a, b) = \arctan\left(\frac{W_i(a, b)}{W_r(a, b)}\right) \tag{3}$$

where $W_i(a, b)$ and $W_r(a, b)$ are the imaginary part and the real part of $W(a, b)$, respectively.

The suggested automated retina diagnosis system is performed according to the following stages. The adaptive histogram equalisation technique is applied to the retina digital image to minimise the non-uniform lighting. Then, the retina image is converted to two

doi: 10.1049/htl.2014.0068

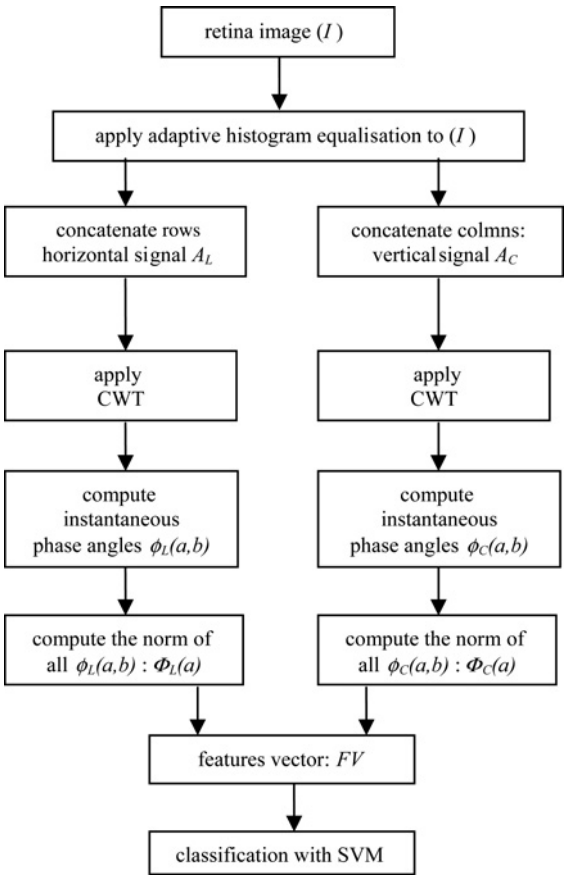

Figure 1 *Flowchart of the proposed retinal automated diagnosis system*

one-dimensional signals: one is formed by the concatenation of the rows and the other one is formed by the concatenation of the columns. Subsequently, each signal is analysed by using the CCWT at a finite number, p, of level decompositions. Following that, the instantaneous phase angles of each one-dimensional signal are computed at each level of decomposition to form one vector, and the norm (magnitude) of this vector is calculated. As a result, the final features vector contains $2p$ (2 one-dimensional signals $\times$ p norms) magnitudes. Finally, the features vector forms the input to the SVM to perform the classification task. The block diagram of the overall automated system is described in Fig. 1.

Let I be an image of size $m \times n$. After applying the adaptive histogram equalisation technique to I, the image A is obtained. Then, the rows of A are concatenated to obtain the one-dimensional signal A_{L} of dimension $m \times n$. Similarly, the columns of A are concatenated to obtain the one-dimensional signal A_{C} of dimension $n \times m$. Therefore the instantaneous phase angles of A_{L} and A_{C} at the level of decomposition a (A_{L} and A_{C}) are $\phi_{\mathrm{L}}(a, b)$ and $\phi_{\mathrm{C}}(a, b)$, respectively. Hence, the overall vector of instantaneous phase angles of A_{L} at the level of decomposition a is obtained by computing the following mathematical norm

$$\Phi_{\mathrm{L}}(a) = \sqrt{\sum_{b=1}^{m\times n} \left(\phi_{\mathrm{L}}(a, b)\right)^2} \tag{4}$$

Similarly, the overall vector of instantaneous phase angles of A_{C} at the level of decomposition a is obtained by computing the following mathematical norm

$$\Phi_{\mathrm{C}}(a) = \sqrt{\sum_{b=1}^{m\times n} (\phi_{\mathrm{C}}(a, b))^2} \tag{5}$$

It is well known [9] that the wavelet scale value a is related to the corresponding frequency F_a according to

$$F_a = \frac{F_C}{a\Delta} \tag{6}$$

where F_C is the wavelet centre frequency and Δ is the sampling period. This relationship indicates that lower values of the scale parameter a correspond to higher values of F_a. Since it can be observed that the presence of retina pathologies is usually associated with specific patterns in the corresponding images, and that these patterns usually involve more or less abrupt variations in the images. Although other choices could have been made, we have concentrated our analysis on the lower scale values $a = 1, 2, 3$.

Hence, the feature vector FV is composed as follows

$$\mathrm{FV} = [\,\Phi_{\mathrm{L}}(1) \quad \Phi_{\mathrm{L}}(2) \quad \Phi_{\mathrm{L}}(3) \quad \Phi_{\mathrm{C}}(1) \quad \Phi_{\mathrm{C}}(2) \quad \Phi_{\mathrm{C}}(3)\,] \tag{7}$$

Vector FV forms the input to the classifier; namely the SVM [8]. This classifier solves a binary classification problem in which the output $y \in \{-1, +1\}$ is obtained by seeking a hyper-plane $w \cdot \Theta(x) + b = 0$ to separate the data from classes $+1$ and -1 with a maximal margin. Here, x denotes the input feature vector, w is a weight vector, Θ is the mapping function to a higher dimension and b is the bias used for the classification of samples. The decision frontier is given by

$$f(x) = \sum_i y_i \alpha_i \Theta(x_i) \cdot \Theta(x) + b \tag{8}$$

where each α_i is a Lagrange coefficient. As mentioned before, the role of the kernel function is to implicitly map the input vector into a high-dimensional feature space to achieve better separability. Finally, the optimal decision separating function can be obtained as follows:

$$y = \mathrm{sign}\left(\sum_i y_i \alpha_i K(x_i, x) + b\right) \tag{9}$$

In this Letter, the quadratic kernel is used to map the input vector

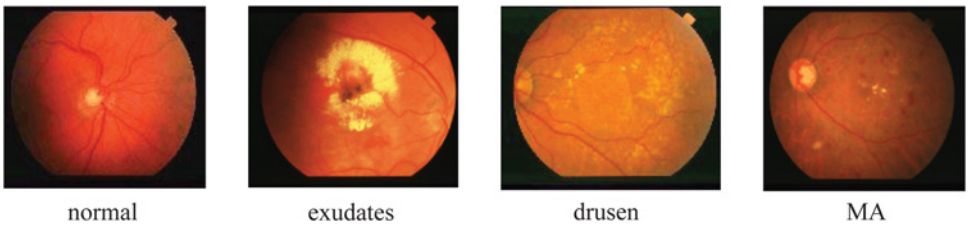

Figure 2 *Examples of retina digital images*

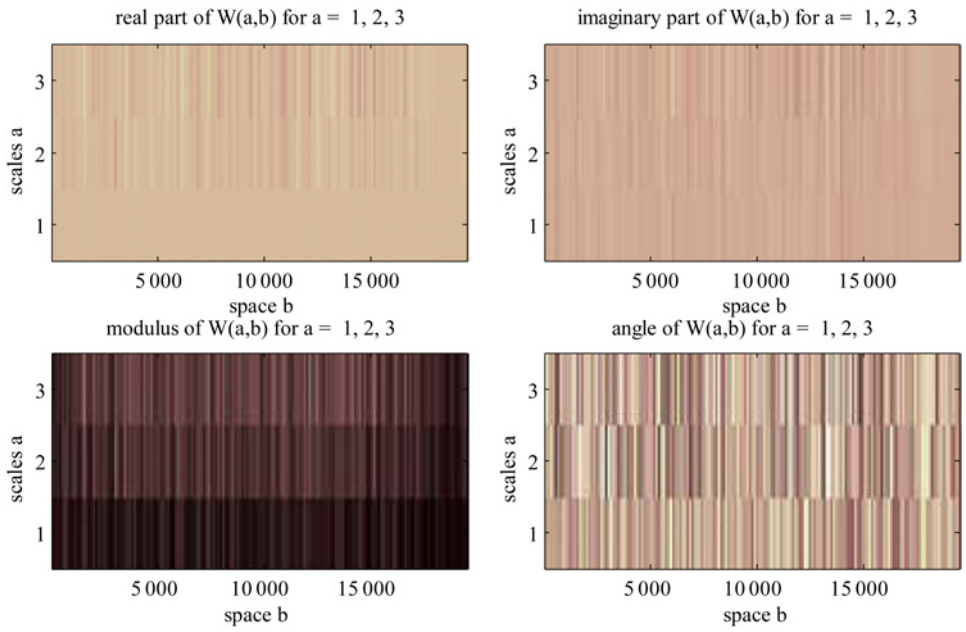

Figure 3 *CCWT representation of the horizontal signal A_L of a normal image*

FV into the high-dimensional feature space. It is given by

$$K(x, x_i) = \Theta(x_i)\Theta(x) = \left((x_i \cdot x) + 1\right)^2 \tag{10}$$

The main advantage of the quadratic kernel is that it belongs to the polynomial kernels family; thus it is a global kernel. In addition, it is less computationally demanding than higher order polynomial kernels and radial basis kernel.

3. Data and simulation results: The dataset is formed by 23 normal, 22 exudates, 20 drusen and 24 MA; all obtained from the STARE database [11]. The LOOM technique is used for better generalisation capability of the SVM. Examples of retina digital images are shown in Fig. 2. Fig. 3 shows the CCWT representation (real part, imaginary part, modulus or magnitude, and angle) of the horizontal signal A_L of the normal image. Similarly, Fig. 4 shows the CCWT representation (real part, imaginary part, modulus or magnitude, and angle) of the horizontal signal A_L of the MA. The modulus (magnitude) of the signals A_L is drawn for comparison purposes with the angle signals. For instance, phase angle signals seem to contain more information regarding the original signal than the modulus. This finding could be explained by the fact that the phase image (signal) reflects the geometrical structure of the texture. Figs. 5–10 show the boxplots of the angle and the phase for normal, MA, drusen and exudate images depending on the CWT level of decomposition for both horizontal and vertical signals. As can be seen, there are clear differences in statistical distributions of the angle and the phase between normal, MA, drusen and exudate images for all decomposition levels, particularly for MA and exudates based on horizontal signals.

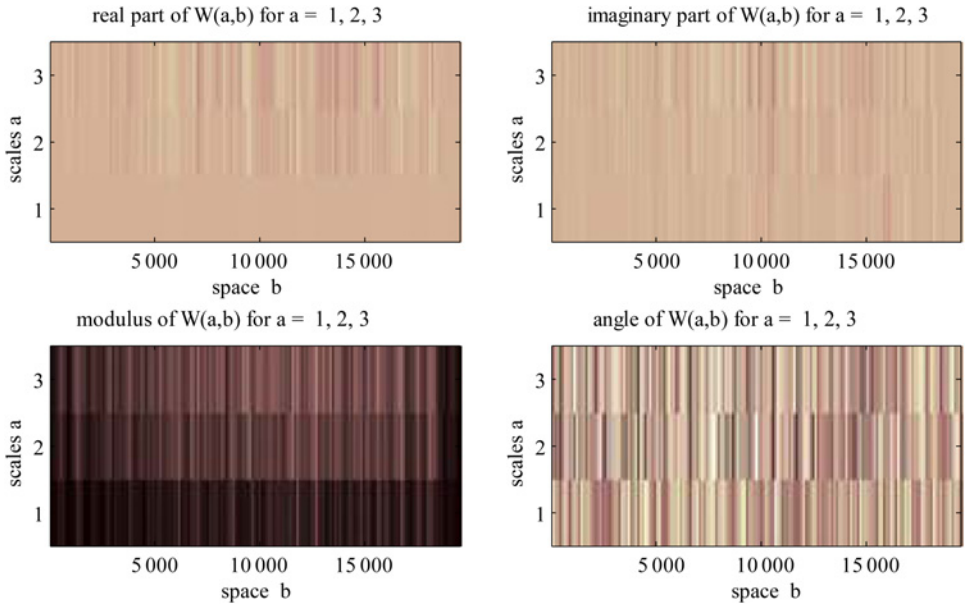

Figure 4 *CCWT representation of the horizontal signal A_L of an MA image*

doi: 10.1049/htl.2014.0068

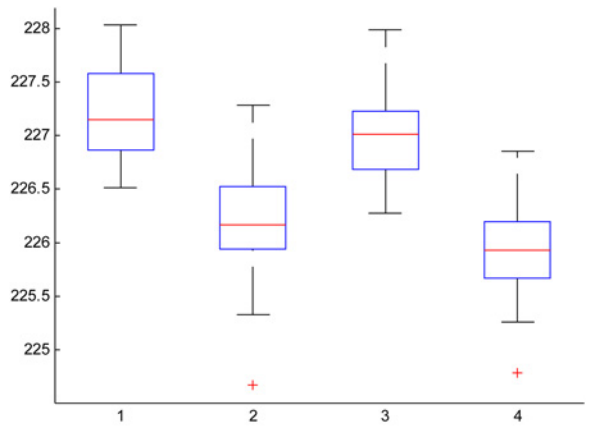

Figure 5 *Boxplot of the horizontal signal A_L phase angle at the first level of decomposition, normal (1), MA (2), drusen (3), exudates (4)*

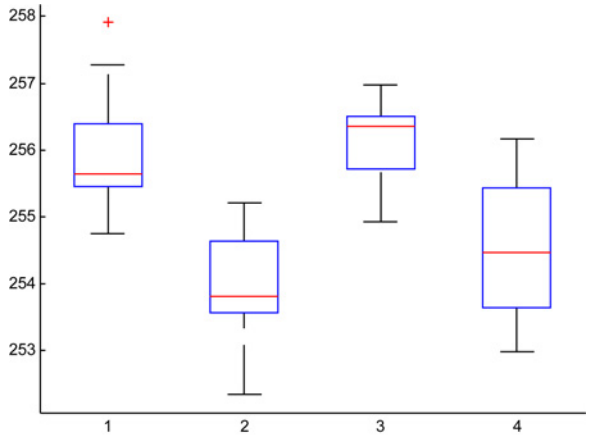

Figure 6 *Boxplot of the horizontal signal A_L phase angle at the second level of decomposition, normal (1), MA (2), drusen (3), exudates (4)*

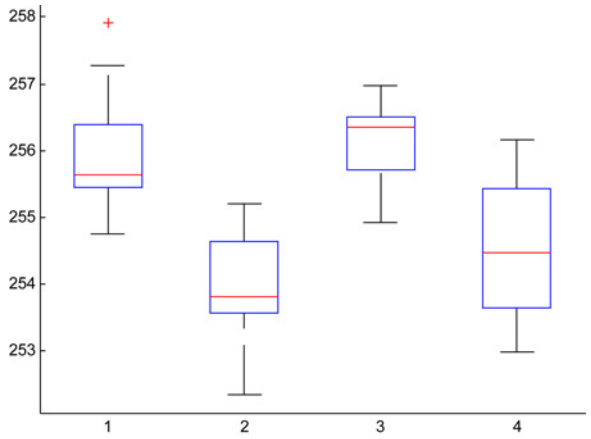

Figure 7 *Boxplot of the horizontal signal A_L phase angle at the third level of decomposition, normal (1), MA (2), drusen (3), exudates (4)*

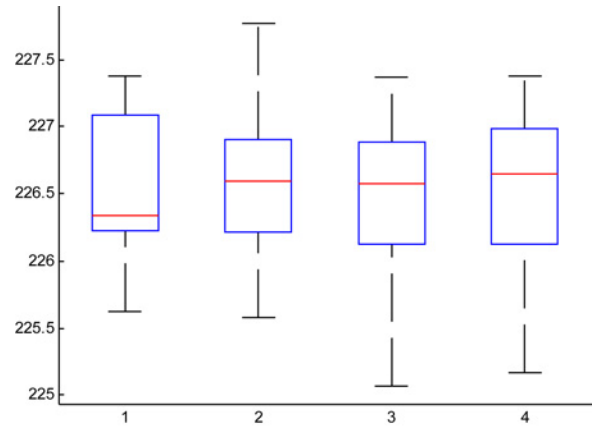

Figure 8 *Boxplot of the vertical signal A_C phase angle at the first level of decomposition, normal (1), MA (2), drusen (3), exudates (4)*

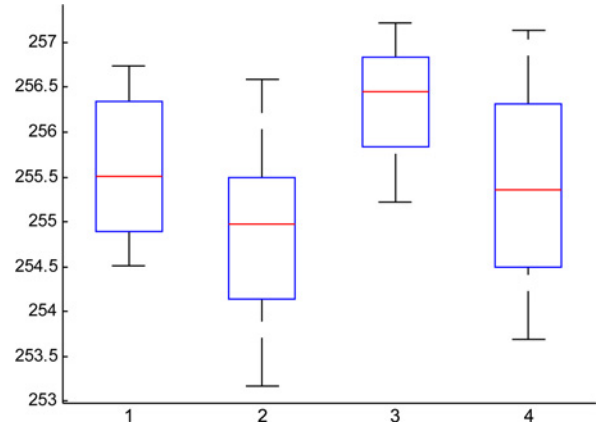

Figure 9 *Boxplot of the vertical signal A_C phase angle at the second level of decomposition, normal (1), MA (2), drusen (3), exudates (4)*

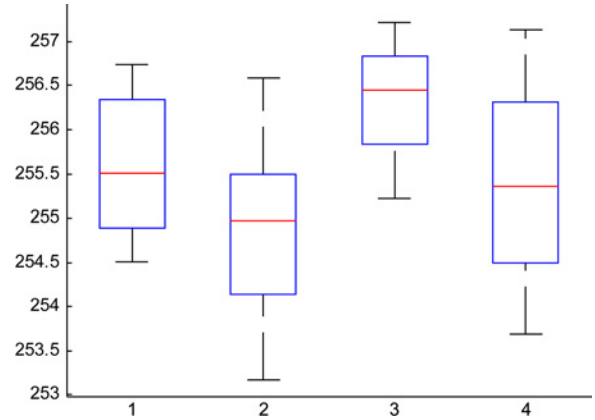

Figure 10 *Boxplot of the vertical signal A_C phase angle at the third level of decomposition, normal (1), MA (2), drusen (3), exudates (4)*

Table 1 SVM simulation results

Statistics	Drusen	Exudates	MA
accuracy	86 (±0.0915)	97 (±0.0431)	100
sensitivity	82 (±0.1276)	100	100
specificity	91 (±0.0635)	94 (±0.0904)	100

This finding could explain the perfect accuracy for MA images and the high accuracy for exudates, as seen in experimental results. For instance, such differences in feature distributions help SVM to separate normal and MA features.

The correct classification rate (accuracy), sensitivity and specificity statistics are used to assess the performance of our approach. Table 1 provides the normal-against-one classification results in percentage and standard deviations are in parenthesis. For simplicity, only the best performances are presented. For instance, results of exudates and drusen in Table 1 are obtained with a polynomial kernel of order 3, while results of MA are obtained with a polynomial kernel of order 2.

As shown in Table 1, our results compare favourably with the results obtained by other algorithms found in the literature to detect exudates [1, 2], drusens [3, 4] and MA [5, 6], especially for MA pathology. The main advantages of our approach are that it is simple, fast and effective. Indeed, it is simple because it does not require segmentation or morphological operations. In addition, image processing and feature extraction based on our approach is fast since the image is transformed into two one-dimensional signals from which phase angles are easily computed to characterise the image with only two features. In particular, the processing time for a given image including concatenation, analysis by CWT and feature extraction has been found to be less than 5 s using Matlab© environment. Finally, our system is accurate because it achieves better pathologies recognition rate results than those reported in the literature for several previous works. However, our proposed method suffers from the following limitation: as it is based on CWT, it is difficult to determine the most appropriate complex wavelet and the most appropriate levels of decomposition of this wavelet. Optimally chosen wavelet and decomposition levels may improve exudates and drusen detection rates.

4. Conclusion: We have presented a new automated system for pathologies detection in retina digital images based on the analysis of the image by means of the CCWT to obtain phase angle information which is fed to SVM. The simulation results show that our method gives results that compare favourably with the results reported in [1–6]. This could be explained mainly by the fact that phase angles contain valuable information that allows discriminating between normal and abnormal retina images. Our automated diagnosis system does not require performing the detection on a given colour channel, segmenting vessel and optic nerve, and also does not use retina morphological features. In summary, the proposed detection system appears to be promising for clinical applications. Future work will consider a larger database and other retina pathologies. We will also investigate the role of complex wavelet type and decomposition levels in improving performance measures.

5 References

[1] Mookia M.R., Acharya U.R., Chua C.K., Lim C.M., Ng E.Y., Laude A.: 'Computer-aided diagnosis of diabetic retinopathy: a review', *Comput. Biol. Med.*, 2013, **43**, (12), pp. 2136–2155

[2] Zhang X., Chutatape O.: 'Detection and classification of bright lesions in colour fundus images'. Proc. of IEEE ICIP, Singapore, 2004, pp. 139–142

[3] Fleming D.A., Philip S., Goatman A.K., *ET AL.*: 'Automated detection of exudates for diabetic retinopathy screening', *Phys. Med. Biol.*, 2007, **52**, (24), pp. 7385–7396

[4] Remeseiro B., Barreira N., Calvo D., Ortega M., Penedo M.G.: 'Automatic drusen detection from digital retinal images: AMD prevention', *Lect. Notes Comput. Sci.*, 2009, **5717**, pp. 187–194

[5] Mora A., Vieira P., Fonseca J.: 'Advances in image processing techniques for drusen detection and quantification in fundus images'. Emerging Trends in Technological Innovation, Int. Federation of Information Processing (IFIP) Advances in Information and Communication Technology, Springer Berlin Heidelberg, 2010, vol. **314**, pp. 299–307

[6] Agurto C., Murray V., Barriga E., *ET AL.*: 'Multiscale AM-FM methods for diabetic retinopathy lesion detection', *IEEE Trans. Med. Imaging*, 2010, **29**, (2), pp. 502–512

[7] Ram K., Joshi G.D., Sivaswam J.: 'A successive clutter-rejection-based approach for early detection of diabetic retinopathy', *IEEE Trans. Biomed. Eng.*, 2011, **58**, (3), pp. 664–673

[8] Vapnik V.: 'Statistical learning theory' (Wiley, New York, USA, 1998)

[9] Mallat S.: 'A wavelet tour of signal processing' (Academic Press, 1999)

[10] http://www.ces.clemson.edu/~ahoover/stare/

[11] Abry P.: 'Ondelettes et turbulence. Multirésolutions, algorithmes de décomposition, invariance d'échelles' (Diderot, Paris, 1997)

doi: 10.1049/htl.2014.0068